Megahertz-Sampled Observations of AC Level 2 Onboard Electric Vehicle Charging

Chad E. Kennedy and Richard D. Kirby, *Schweitzer Engineering Laboratories, Inc.*

***Abstract*—The rapidly increasing number of electric vehicles (EVs) and other nonlinear loads, such as LED lighting, within the U.S. presents a potential challenge to the distribution grid. Nonlinear loads, such as single-phase EV chargers, convert ac power to dc power through solid-state switching, which can cause voltage fluctuations, reduced capacity, and increased losses. Industry standards define limits for low-frequency harmonic currents but do not address higher frequency noise.**

This paper presents observations for a 240 V, 32 A Level 2 EV charger using 1 Msps time-series data and provides a method for accurate power and energy measurements for all signal shapes. The high-resolution power quality analysis includes time-domain energy packet accumulation. Charts and calculations provide reference.

I. Introduction

Electric vehicle (EV) sales make up an increasing portion of new auto sales. In 2022, 5.8 percent of new cars purchased in the U.S. were EVs, which is up from 3.2 percent in 2021. Projections estimate that by 2030, over 26 million EVs will be on U.S. roadways [1] [2]. The rapid adoption of EVs raises concerns about the demand on power systems and the power quality effects of large nonlinear load growth.

This paper discusses the potential power quality impact of high-current switching EV charging for a single 240 V, 32 A Level 2 EV charger and investigates whether it creates significant current harmonics or signal distortion beyond the 2.4 kHz limit set by IEC 61000-3-12 [3]. Although 1 million samples per second (Msps) power quality meters have existed since the 1980s, no field data analyses of the power system effects of EV chargers above 2.4 kHz are presented in published papers.

We observe the voltage and current signals of a Level 2 EV charger using a 1 Msps time-series data set. This sample rate captures signals every microsecond to better visualize zero crossings, waveform peaks, load switching, and high-frequency noise. Traditional harmonic calculations help quantify baseline frequency performance for lower-order harmonics to the 40th order, or 2.4 kHz on a 60 Hz system. This paper also analyzes 1 µs time-domain power and 1 ms energy calculations that provide better resolution for nonsinusoidal signals than traditional 1-cycle power calculations.

Section II describes how the waveform recorder samples and records the raw current and voltage waveforms [4]. Section III evaluates the Level 2 EV charger harmonic current draw against the IEC 61000-3-12 standard with frequency-domain data. Section IV examines the raw current and voltage waveform data at two different sample rates. Sections V and VI discuss time-domain power and energy results and describe the benefits provided by these calculations for nonlinear systems.

II. Signal Sampling and Processing

The waveform recorder directly samples a single-phase 240 V system connected to a 32 A Level 2 charger, as shown in Fig. 1. At IAX and IBX, the recorder samples the current. At VA and VB, the recorder monitors the voltages L1-N and L2-N, respectively. The charging current is set to 15 A to allow direct connection through the waveform recorder.

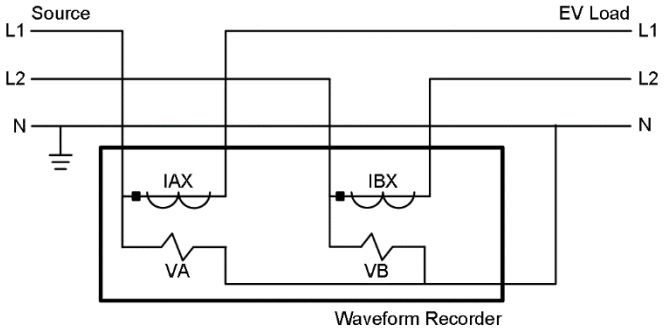

Fig. 1. Metering diagram

Time-series waveform captures of 1.2 seconds at 10 kilo samples per second (ksps) and 1 Msps are stored as event report files for offline analysis. The 1 Msps data provide high-resolution sampling for analyzing solid-state, power conversion switching devices and the 10 ksps data demonstrate data rates captured by traditional recording devices.

The waveform recorder uses fixed time-based sampling that prefilters analog currents and voltages with an analog low-pass filter to avoid aliasing. The 1 Msps signals have an effective measurement bandwidth of 400 kHz with an 18-bit analog-to-digital converter resolution [4]. The signals are then time-stamped to the microsecond. Available 10 ksps sample signals have an effective measurement bandwidth of approximately 3 kHz. Waveform captures are stored in a COMTRADE file format. All quantities in this paper originate from the instantaneous samples of the current and voltage waveforms recorded at 1 Msps, unless otherwise noted. The analog samples are captured over a 1.2-second window.

III. Low-Frequency Harmonic Observations

An harmonic analysis using the Fourier Transform provides insight into the frequency characteristics of the charger. The spectrum shown in Fig. 2 illustrates the contribution of each discrete harmonic to the measured load.

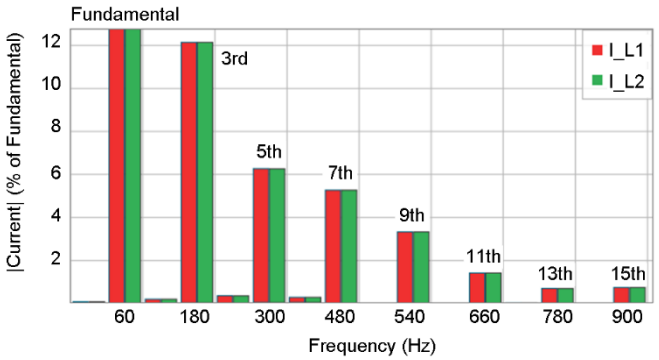

Fig. 2. Current harmonics from Level 2 charger

The IEC 61000-3-12 standard presents practical limits for conducted harmonics from equipment with a current draw of 16 to 75 A, including EV battery chargers. This standard defines harmonic limits dependent on the short-circuit ratio (Rsce), which is the ratio of the short-circuit apparent power to the apparent power of the equipment. While a 15 A load is typically covered by IEC 61000-3-2, this paper uses IEC 61000-3-12 based on the 32 A full-rated current of the Level 2 charger. An additional analysis at the full charging current is needed to verify conformance to IEC 61000-3-12.

The current harmonic limits shown in Table I are the allowable limits of IEC 61000-3-12. This analysis uses an Rsce of 33, which is the most stringent set of limits and is suitable for all interconnection locations on a power system. The total harmonic distortion (THD) calculation uses harmonic content to the 40th order, or 2.4 kHz. Table I also summarizes the measured harmonic components of the Level 2 EV charger.

TABLE I
ALLOWABLE AND MEASURED CURRENT HARMONIC PERCENTAGE LIMITS

Harmonic	**I_3**	**I_5**	**I_7**	**I_9**	**I_{11}**	**I_{13}**	**THD**
Limit %	22	11	7	4	3	2	23
Measured %	12	6	5	4	3	1	15

The Level 2 charger harmonic measurements are at or below the limits of the standard, including the current THD of 15 percent. Because the standard measures compliance to the 13th harmonic order for discrete harmonics and the 40th order for THD, it is worth assessing the load for high-frequency switching and noise. This analysis requires higher sample rate data captures and benefits from the time-domain analysis that supplements the frequency-domain analysis.

IV. HIGH SAMPLE RATE OBSERVATIONS

Measuring the current and voltage at 1 Msps and observing the waveforms provides a depth of insight that is not visible in the harmonic histogram. The current waveform in Fig. 3 displays considerable distortion.

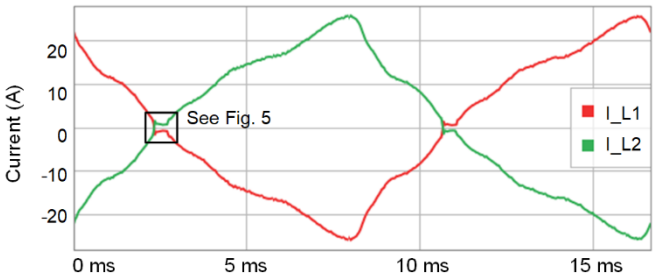

Fig. 3. 1 Msps current waveform

The voltage signals in Fig. 4 have a small amount of distortion, which is shown by the slight flattening towards the peaks. This distortion may be caused by the current peak.

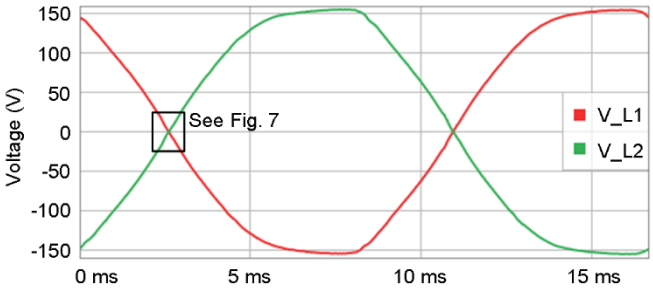

Fig. 4. 1 Msps voltage waveform

The 800 µs window shown in Fig. 5 highlights a distorted current signal that flattens at the zero crossing of the waveform. There is a 30 µs overshoot immediately following the zero crossing, which leads to a 1.0 A magnitude flat-lined current waveform for 300 µs.

Power electronics frequently include two polarized high-current switching transistors with controls that prevent both transistors from driving current into the circuit at the same time. The zero-crossing current responses are a likely result of this circuit.

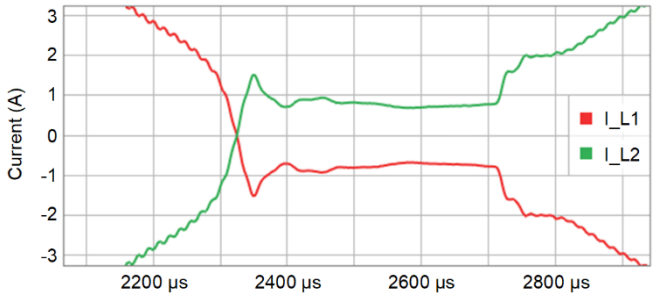

Fig. 5. 1 Msps current zero crossing

There is a noticeable difference in the behavior of the 1 Msps signals in Fig. 5 and the 10 ksps signals in Fig. 6. The 10 ksps sample rate recording loses much of the signal detail and appears closer to an ideal sinusoid. A typical frequency-based power quality meter may have a sample rate of 512 to 1,024 samples per cycle (spc) and would similarly lose much of the signal fidelity.

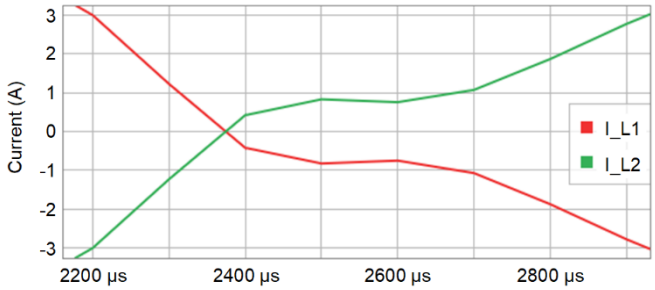

Fig. 6. 10 ksps current zero crossing

The voltage waveform in Fig. 7 displays a zero crossing with limited distortion and clean transitions. The voltage plateaus at 22.4 V, which is coincident with the current zero crossing. This suggests that the current load slightly affects the source voltage.

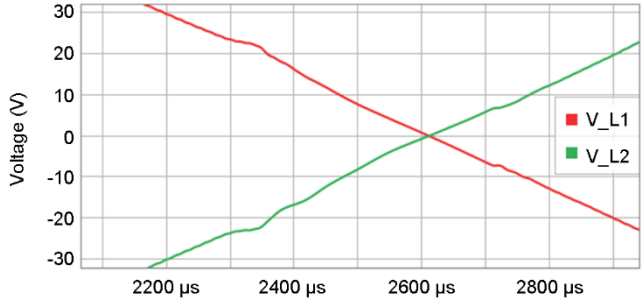

Fig. 7. Msps voltage zero crossing

The 6 ms windows in Fig. 8 and Fig. 9 show current peaks that lag the voltage peaks, which is expected for a slightly inductive load. A small-magnitude, high-frequency ripple on the current signal is noticeable and discussed in Section V. The voltage peak is slightly flattened compared to a perfect sinusoid, which is likely caused by the load current.

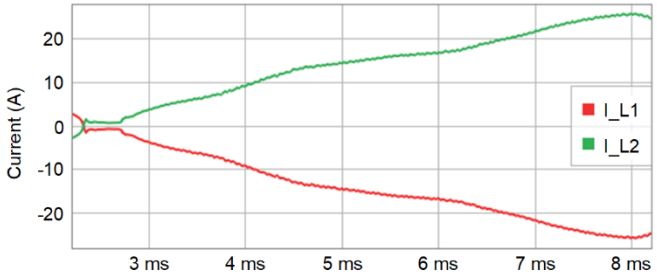

Fig. 8. 6 ms, 1 Msps current waveform

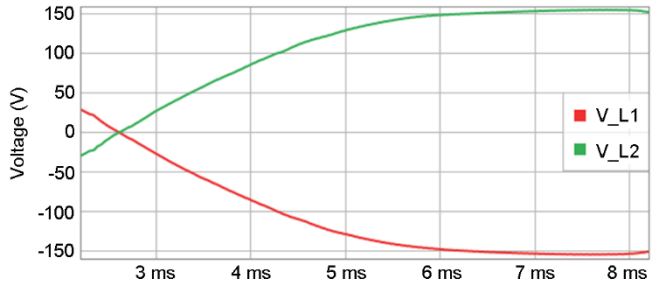

Fig. 9. 6 ms, 1 Msps voltage waveform

While the current and voltage waveforms show some nonlinearity, the high-frequency analysis did not reveal significant distortion beyond the initial frequency-domain analysis. This provides some reassurance to retailers and distribution utilities that the IEC 61000-3-12 or similar standards capture most of the distortion caused by a Level 2 charger. It would be prudent to sample various charger models to determine whether this is consistent across Level 2 chargers.

V. Time-Domain Power

Analyzing the power flow and energy transfer within a power system can provide additional insight into nonlinear load characteristics.

Given the load characteristics of the EV and the potentially varying frequency of the source, a time-domain method for calculating power and energy can provide more repeatable results for differing loads. As noted in Section III, the Level 2 charger waveforms include multiple signal frequencies. The product of the current and voltage as instantaneous power flow provides additional insights.

Instantaneous power is calculated as the product of each current and voltage sample [k] (1) and then separated into positive (2) and negative (3) components.

$$p[k] = v[k] \bullet i[k] \tag{1}$$

$$p^{POS}[k] = \begin{cases} p[k], p[k] > 0 \\ 0, \text{otherwise} \end{cases} \tag{2}$$

$$p^{NEG}[k] = \begin{cases} p[k], p[k] < 0 \\ 0, \text{otherwise} \end{cases} \tag{3}$$

Separating the positive and negative instantaneous power components into two terms provides insight into the efficiency of the energy exchanged between the source and load. If 100 percent of the energy transfer is positive, then the current and voltage have the same polarity and the energy is fully consumed at the load. If 50 percent of the energy transfer is positive and 50 percent is negative, then the energy is oscillating between the source and load with no actual consumption.

Average power calculations can vary between measurement instruments, including a 1-cycle method or moving-window averages. This paper does not define average power and uses P_AV in Fig. 10 for illustration.

Fig. 10 captures the instantaneous power, p[k]. The instantaneous power exposes nonlinearities in the metered power where a perfectly linear load would appear as an ideal sine wave for a pure sinusoidal input signal. This helps immediately identify nonlinear systems. Frequency-domain data, including the harmonic analysis, can supplement the time-domain analysis and help identify specific disturbance frequencies.

It is also notable how the instantaneous power drops below zero, which indicates that there is bidirectional power flow.

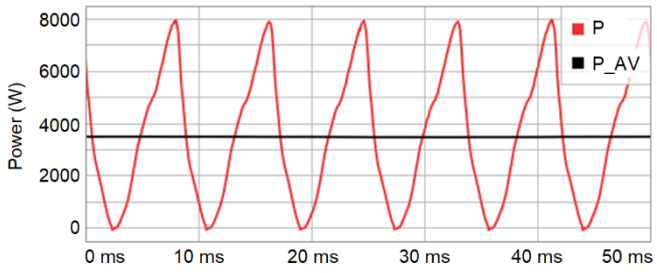

Fig. 10. Instantaneous and average power

Isolating the instantaneous power into positive and negative terms provides insight into the load characteristics. Fig. 11 shows the positive power, $p^{POS}[k]$, and Fig. 12 shows the negative power, $p^{NEG}[k]$.

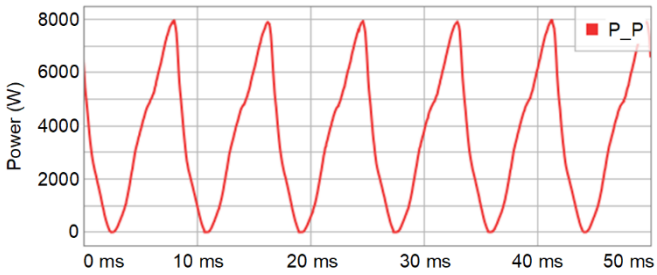

Fig. 11. Positive power $p^{POS}[k]$

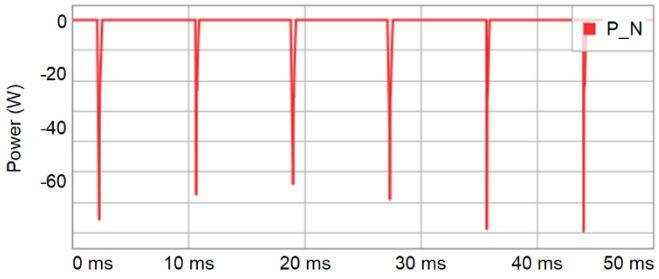

Fig. 12. Negative power $p^{NEG}[k]$

As seen in Fig. 3 and Fig. 4, the load current and voltage zero crossings are nearly time-aligned. In fundamental, single-frequency terms, the current and voltage are in phase. Therefore, we expect most of the instantaneous power to be positive with little to no negative power. Because the load is nonlinear, it is easier to assess the positive and negative power in the time domain.

In Fig. 11, the positive power peaks at 7,900 W. In Fig. 12, the negative power peaks at –70 W. The charger and battery consume most of the power and only a small amount of power returns to the source. The large amount of positive power and the small amount of negative power are consistent with power electronics that contain power factor correction circuits.

The 300 µs window shown in Fig. 13 reveals a high-frequency ripple of approximately 15.6 µs in the instantaneous power.

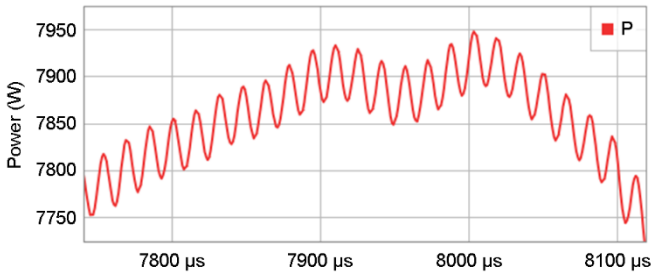

Fig. 13. Instantaneous power ripple

The spectral analysis of the L1 and L2 currents shown in Fig. 14 and Fig. 15 confirms a 64 kHz disturbance with an amplitude 50 dB below the fundamental current. The ripple is approximately 60 W in amplitude added to a total peak load of 7,900 W. The 64 kHz ripple is consistent with high-frequency ac-to-dc switching conversions that are common in power electronics. The 64 kHz ripple is most likely caused by the switching frequency of the Level 2 EV charger. Inductive filtering within the charger likely smooths the current signal and limits the ripple to 60 W.

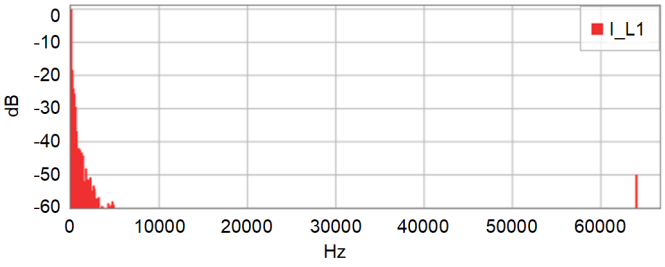

Fig. 14. Spectral analysis of L1 current signal

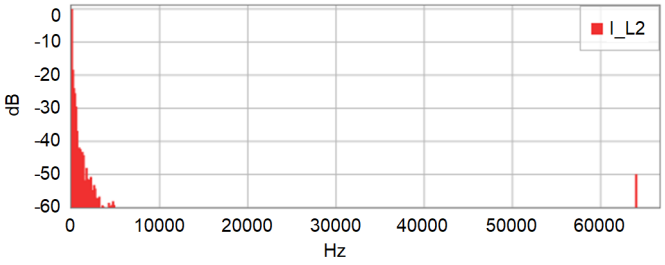

Fig. 15. Spectral analysis of L2 current signal

VI. Time-Domain Energy

For nonlinear loads, energy accumulation provides additional insight into the bidirectional energy transfer between the source and the load. The instantaneous power analysis indicates that the Level 2 charger produces a small amount of negative power flow back to the source. Integrating this power over time quantifies the exact amount of energy transferred and consumed by the load compared to how much energy the load returned to the source.

Integrating power over precise and deterministic periods of time produces energy packets. Net energy is the difference between the positive and negative energy in a discrete

period (4). Like instantaneous power, energy packets can be separated into positive (5) and negative (6) terms.

$$E^{NET}[n] = T_S \sum_{k=M(n-1)+1}^{k=Mn} p[k] \quad (4)$$

$$E^{POS}[n] = T_S \sum_{k=M(n-1)+1}^{k=Mn} p^{POS}[k] \quad (5)$$

$$E^{NEG}[n] = T_S \sum_{k=M(n-1)+1}^{k=Mn} p^{NEG}[k] \quad (6)$$

Simply stated: "Energy packets are precise measurements of energy exchanges, independent of system frequency and phase angles, and are computed and communicated at a fixed rate, with a common time reference" [5].

Power analysis software integrates 1,000 samples of 1 µs data into a 1 ms energy packet [5] [6]. The analysis calculates joules (watt seconds) of energy packets exchanged every 1 ms. For example, a 1-watt load consumes 1 millijoule of energy within a 1 ms period. Energy packets are calculated in the SI unit joules (J). Joules are converted into watthours (Wh) by a time-scaled 3,600 seconds per hour where 1 Wh equals 3,600 J.

This analysis uses 1 ms intervals for calculating net (7), positive (8), and negative (9) energy packets from 1 µs raw samples. With T_S = 1 µs and M = 1,000, 1 ms energy packets are:

$$E^{NET}_{1\,ms}[n] = 1\,\mu s \bullet \sum_{k=1000(n-1)+1}^{k=1000n} p[k] \quad (7)$$

$$E^{POS}_{1\,ms}[n] = 1\,\mu s \bullet \sum_{k=1000(n-1)+1}^{k=1000n} p^{POS}[k] \quad (8)$$

$$E^{NEG}_{1\,ms}[n] = 1\,\mu s \bullet \sum_{k=1000(n-1)+1}^{k=1000n} p^{NEG}[k] \quad (9)$$

The 1 ms energy packet charts in Fig. 16, Fig. 17, and Fig. 18 resemble the instantaneous power plots integrated into discrete windows. The net energy plot displays the sum of positive and negative energy packets in a 1 ms interval. The positive and negative plots separate the energy into independent directional components: positive energy flowing into the load and negative energy flowing out of the load.

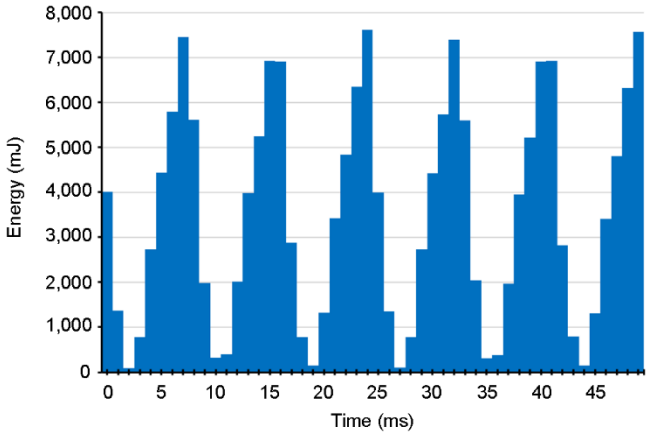

Fig. 16. Net 1 ms energy packets

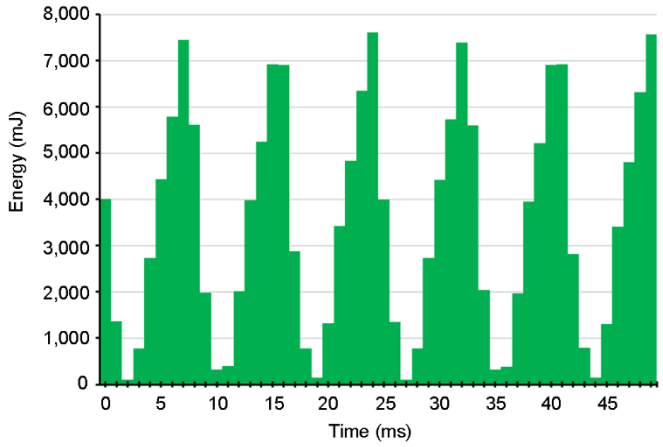

Fig. 17. Positive 1 ms energy packets

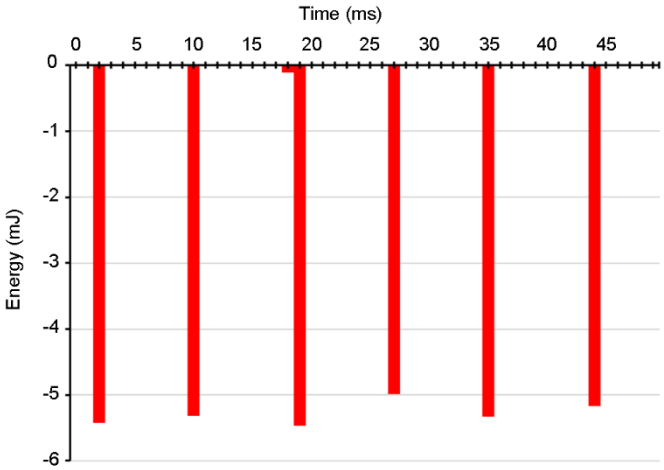

Fig. 18. Negative 1 ms energy packets

The fixed time-domain numerical integration calculation of energy has multiple advantages over variable frequency-based calculations of 1-cycle power and energy calculations. The first advantage is that a deterministic integration period allows sample-by-sample comparison of data rather than measuring energy consumption over a nondeterministic period with a variable period.

The second advantage of time-domain energy integration is the elimination of frequency tracking as long as the integration period is significantly smaller than the signal period. Energy packet integration windows can update over virtually any window, while frequency-dependent integration windows can vary each cycle. Time-domain energy packets measure variable energy over a fixed time interval rather than variable energy over a variable frequency period. This becomes especially valuable for signals with small signal-to-noise ratios and is valid for any signal type, including dc, where frequency is hard to determine.

Traditional energy meters integrate energy over periods of 1 cycle, 12 cycles at 60 Hz (~200 ms), or longer. These meters use one of many different methods to calculate reactive power and reactive energy, which are reported as VARs and VARh, respectively. The VAR is a nonphysical construct that does not measure watts of power or joules of energy. The calculation results from different meter models can vary significantly when

metering nonlinear systems, which causes issues with repeatable and reproducible results.

The third advantage of time-domain energy integration over 1 ms is that positive and negative energy exchanges become visible, are deterministic, and are measurable in real units of watts and joules.

Table II shows the summation of energy across 600 ms and 1.2 s intervals. To measure any negative energy, the integration interval should be greater than one-half-cycle of the fundamental period, such as 10 ms for a 60 Hz system.

TABLE II
ENERGY PACKET SUMMATION

Interval (µs)	E^{NET} (J)	E^{POS} (J)	E^{NEG} (J)
600,000	2,093	2,094	–0.4
1,200,000	4,187	4,188	–0.8

Row two is approximately double row one for each of the energy packet calculations, as expected, which demonstrates the accuracy, repeatability, and granularity when metering a load over a short interval.

Like the instantaneous power calculations, the time-domain energy analysis confirms that the load consumes most of the power transferred from the source. The data confirm that the charger is only slightly inductive or capacitive and suggests that it includes power factor correction.

These data do not provide insight into how much energy the charger converts into dc power, which charges the battery. Future experimentation could capture dc current and voltage measurements and calculate ac-to-dc power conversion efficiency.

VII. CONCLUSION

The low-frequency harmonic analysis of the Level 2 EV charger suggests compliance with the limits set by the industry standard of IEC 61000-3-12. Multiple chargers on a common distribution circuit will cause additive nonlinear distortion that this paper did not address.

The Level 2 charger draws approximately 60 W of nonsinusoidal power above 2.4 kHz, as observed by the 64 kHz ripple. While the 64 kHz ripple power levels are moderate, the higher frequency analysis of switching power supplies may become an important measurement to reduce conducted emissions disturbances on distribution systems.

The traditional power measurement instrumentation with 512 to 1,024 spc rates does not capture the high-frequency ripple from some switching power converters. Adding Msps sample rate devices to the distribution system can help identify high-frequency disturbances as the number of power conversion devices, such as high-current EV chargers, grows.

The time-domain power and energy analyses provide precise insight into the load characteristics, regardless of the shape of the signal. This analysis shows that the Level 2 charger, while nonlinear, does not create significant negative energy that is returned to the source. Analyzing the dc power output can supplement this analysis with a power conversion efficiency calculation.

The expansion of high-resolution, time-domain measurement and analysis techniques provides additional insights into opportunities to improve efficiency, increase system capacity, and better control energy moving at the speed of light.

VIII. REFERENCES

[1] "EEI Projects 26 Million Electric Vehicles Will Be on US Roads in 2030." Available: eei.org/News/news/All/eei-projects-26-million-electric-vehicles-will-be-on-us-roads-in-2030.

[2] Kelley Blue Book, "New Car Sales Fell in 2022, But New Electric Car Sales Rose Dramatically." Available: kbb.com/car-news/new-car-sales-fell-in-2022-but-new-electric-car-sales-rose-dramatically/.

[3] IEC Std. 61000-3-12:2011, *Electromagnetic compatibility (EMC) - Part 3-12: Limits - Limits for harmonic currents produced by equipment connected to public low-voltage systems with input current > 16 A and ≤ 75 A per phase*.

[4] *SEL-T400L Time-Domain Line Protection Instruction Manual*. Available: selinc.com.

[5] E. O. Schweitzer, III, D. E. Whitehead, G. Zweigle, V. Skendzic, and S. V. Achanta, "Millisecond, Microsecond, Nanosecond: What Can We Do With More Precise Time?" proceedings of the 42nd Annual Western Protective Relay Conference, Spokane, WA, October 2015.

[6] Matthew J. Lewis and Richard D. Kirby, "Energy and Power Measurements on a Nonsinusoidal 345 kV System Using Three-Phase Megahertz Time-Series Data," proceedings of the Annual Georgia Tech Fault and Disturbance Analysis Conference, Atlanta, GA, May 2023.

IX. BIOGRAPHIES

Chad E. Kennedy earned his BS in electrical engineering from the University of Dayton in Dayton, Ohio in 2006. He joined Schweitzer Engineering Laboratories, Inc. (SEL) in 2012 and works as a protection and metering application engineer in King of Prussia, Pennsylvania. Chad has been a local technical support meter expert for the last 8 years. He is an IEEE member.

Richard D. Kirby is a senior engineer at Schweitzer Engineering Laboratories, Inc. (SEL) in Houston, Texas. His focus is time-domain metering, power quality, transient recording, and disturbance detection. He is a registered Professional Engineer in Arkansas, Louisiana, Michigan, Oklahoma, and Texas. He has 31 years of diverse electric power engineering experience. He received a BS in engineering from Oral Roberts University in Tulsa, Oklahoma, in 1992, and in 1995, he earned his Master of Engineering in electric power from Rensselaer Polytechnic Institute in Troy, New York. He is a senior member of the IEEE Power & Energy Society and the IEEE Industrial Applications Society.